Available online at www.sciencedirect.com
SCIENCE DIRECT®
Journal of Magnetic Resonance 176 (2005) 249–256
JMR Journal of Magnetic Resonance
www.elsevier.com/locate/jmr

Communication

Orientational anisotropic studies by field rotation technique: Near zero-field pulsed EPR experiments of pentacene doped in *p*-terphenyl

Jun Lang, David J. Sloop, Tien-Sung Lin *

Department of Chemistry, Washington University, St. Louis, MO 63130-4899, USA

Received 25 February 2005; revised 27 May 2005
Available online 2 August 2005

Abstract

We report a new technique to map the orientational anisotropy of paramagnetic systems without physically changing the crystal orientations in near zero-field (NZF) pulsed EPR experiments. By implementing three sets of orthogonal coils around the sample, we are ble to create a magnetic vector up to 2 mT in any three-dimensional orientation in space. In NZF region, the hyperfine tensor elements are comparable to the electronic Zeeman interaction energy, thus very rich spectral patterns can be obtained by ''dialing'' in a magnetic field vector without moving the sample. The technique further allows us to examine the site symmetry of organic crystals and powdered solids doped with chromophores which can be photo-excited to the triplet state by laser light. The technique is exemplified in the study of pentacene in *p*-terphenyl crystals.

Keywords: Pulsed EPR; Near zero-field; Field rotation technique; Triplet state; Organic crystals

1. Introduction

Previously, we reported a zero-field (ZF) pulsed electron paramagnetic resonance (EPR) study of the photo-excited triplet state of pentacene in mixed crystal systems [1]. The spin dipolar interaction between two electron spins of the $S = 1$ system gives rise to the ZF splitting. The populations to the spin sublevels of the photo-excited triplet states of organic molecules are selective and deviated from the Boltzmann distribution law. The selective population to the triplet sublevels arises from the symmetry-restricted spin–orbital coupling of the system. We take advantage of high electron spin polarization created in the photo-excitation of organic triplet states in our ZF experiments. By applying a microwave pulse a short time after a laser excitation with proper pulse duration and frequency, we create magnetic moments in the photo-excited triplet state, which evolve with time. We then detect the free induction decay (FID) signals in ZF. The observed spectral line widths are typically narrower than 700 kHz. The transitions among these spin sublevels in ZF can be measured with an accuracy of 10 kHz. Here, we report the spectral patterns at near zero-field (NZF) region up to 1 mT. The systems we have studied are the photo-excited triplet state of perdeuterated pentacene-d_{14} in *p*-terphenyl (PDPT), and pentacene-h_{14} in *p*-terphenyl (PHPT).

The conventional method to study the anisotropy of paramagnetic parameters, such as hyperfine interaction (HFI) and *g* tensor elements is to perform an angular dependence study of spectral positions with respect to the external field by physically rotating the crystal on a goniometer. Alternatively, one may rotate the external field and leave the sample stationary. This method is particularly attractive for NZF experiments. Here we

* Corresponding author. Fax: +1 314 935 4481.
E-mail address: Lin@wustl.edu (T.-S. Lin).

1090-7807/$ - see front matter © 2005 Elsevier Inc. All rights reserved.
doi:10.1016/j.jmr.2005.06.012

report such an alternative method which allows us to map the orientation anisotropy of the photo-excited triplet states in an organic crystal without physically moving the sample. We believe this is a promising experimental technique with the capability of examining the detailed anisotropy of crystal sites and paramagnetic interaction, such as HFI, quadrupole, or other types of interactions in the presence of a magnetic field. The spectral patterns undergo drastic changes when we turn on a magnetic field as small as 0.4 mT where the magnitudes of HFI and the electronic Zeeman interaction are comparable.

2. Experimental

2.1. Samples, laser, and microwave

The solids of *p*-terphenyl purchased from Aldrich were further purified by zone refining. Pentacene and deuterated *p*-terphenyl were also purchased from Aldrich and used as received. Deuterated pentacene was a gift from Dr. D. Wiersma and used as received. Mixed crystals of pentacene doped in *p*-terphenyl were prepared by standard Bridgman technique. Dopant pentacene concentrations were in the range of 10^{-3}–10^{-4} mol/mol. The sample is then placed in the lump circuit coil resonator, which is tunable from 1.3 to 1.5 GHz.

The *p*-terphenyl single crystal (space group $P2_1/a$, 2 molecules/cell) [2,3] was cleaved along the *ab* plane and sliced down to 2 mm thickness. The *b* crystallographic axis was identified by the conoscopic technique. The crystal with the cleavage *ab* plane was mounted on a KEL-F wedge (diameter: 3 mm) which were designed according to the crystal structure data of *p*-terphenyl [2,3]. The crystal *b* axis was then aligned along a marked line on the wedge. For instance, when the crystal is properly mounted on a *xy* wedge, one of the pentacene molecular *z* axis is along the vertical direction (Lab **Z** axis). The molecular axes will be denoted by lower cases *x*, *y*, and *z*, and the laboratory axes by upper bold **X**, **Y**, and **Z**. The powder samples were prepared by grinding the crystals with mortar and pestle.

Avco C950 pulsed nitrogen laser, which emits at 337 nm, was used to optically pump the pentacene molecule into the second excited singlet state. Laser pulse duration is 7 ns, and the repetition rate was set at 1–2 Hz for all the data presented here. The lowest triplet state is populated by intersystem crossing from the lowest excited singlet state. After the laser pulse, microwave pulses at a local oscillator frequency with duration of about 100 ns are fed into the resonator to induce transitions between spin sublevels.

The pulse sequence is generated by a master computer, which contains five 2-channel programmable pulse cards, which makes the console capable of supplying up to 10 independently controlled pulses each repetition. The pulse sequence is also controlled by a program running on the master computer. The B_1 field is applied along the Lab **Z**. We used a simple FID-single microwave pulse sequence in most of the experiments. A 500 ns delay between the laser and microwave pulse was set to avoid picking up noise from the laser. A digitizing oscilloscope is triggered by the laser pulse and starts data acquisition at about 85 ns (the dead time of the spectrometer) after the end of microwave pulse. For the T_y–T_z transition, we applied an additional radio-frequency at 107.4 MHz (the energy gap between T_x and T_y spin substrates) to redistribute the ZF population and to enhance the signal to noise ratio (see Eq. (5) below).

The amplified FID signal is mixed with the local oscillator and digitized. The local oscillator frequency is generally set at about 4 MHz lower than the expected resonance frequency. The signal is, then, fed into the LeCroy 9400A digitizing oscilloscope. The repetitive signals are then averaged 100–200 times by the digitizing oscilloscope. Other experimental conditions were given previously [1].

2.2. Field rotation and control

Magnetic field is controlled by three sets of orthogonal coils with computer controlled currents (see Fig. 1). Two of the three sets are Helmholtz pairs with the coil diameters of 13″ and 9″. They are used to control the field in lab frame **X** axis and **Z** axis, respectively. Hence, they are labeled as coil **X** and coil **Z**, respectively. The spacing between coils of each pair is the same as the coil radius. The third coil, coil Y (in the paper plane), is a single large coil with 25″ diameter, centered at the resonator. The resistances of coil **X**, **Y**, **Z** are 70.5, 22, and 253 Ω, respectively. Coils are each driven by separate computer controlled Xantrex XHR600 programmable power supplies, which can deliver up to 600 V/1.7 A.

The field strength generated by each coil set is given by the following equation

$$B_i = (C_i \times V_i) - B_i', \tag{1}$$

where B_i is the field strength along the axis of coil set i (**X**, **Y**, or **Z**) and B_i' is the residual earth field along the i axis, C_i is field-voltage calibration constant of coil set i, and V_i is the voltage across coil i. The calibration constants are 0.0327, 0.0339, and 0.0233 mT per volt for coil **X**, **Y**, and **Z**, respectively, assuming constant temperature condition generally met by the small field and current. Residual earth magnetic fields along coil axes are −0.024, −0.005, and −0.035 mT, for coil **X**, **Y**, and **Z**, respectively. To obtain a desired field strength at any given orientation (include zero field), we developed a software program written in Visual Basic to determine the field magnitude needed along each axis in the corresponding power supply.

In the spherical polar coordinate system, field components are given as follows:

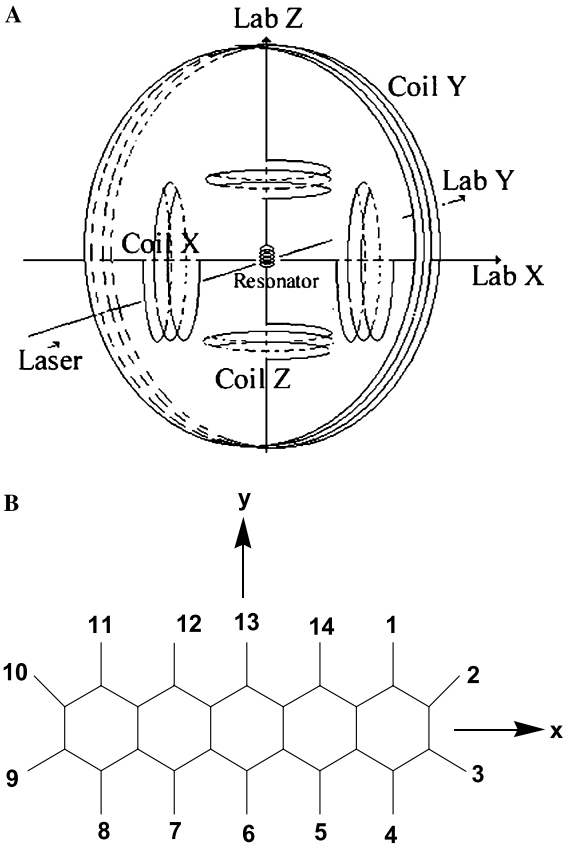

Fig. 1. (A) Laboratory frame axis system and field coil set-up. The large oval pairs are the field controlling Helmholtz pairs for **X** and **Z** axes. A single large circle represents the field controlling coil for **Y**, and (B) molecular axes of the pentacene molecule.

$$B_X = B_0 \sin\theta\cos\phi,$$
$$B_Y = B_0 \sin\theta\sin\phi, \quad (2)$$
$$B_Z = B_0 \cos\theta.$$

For instance, when we need to apply 0.5 mT field at an orientation of $\theta = 137°$ and $\phi = 94°$ in an experiment, the program determines field should be -0.024 mT along **X** ($0.5\,\text{mT} \times \sin 137° \times \cos 94°$), 0.340 mT along **Y**, and -0.365 mT along **Z**. The required voltages across coil **X**, **Y**, and **Z** are determined by Eq. (1). The next step is to deliver the desired voltage settings to each power supply and allow 500 ms settling time for the desired fields. Since the power supplies are not capable of providing a negative voltage, a program was written to manipulate the digital output of Measurement Computing PMD-1208 DAQ USB module when it needs to set a negative voltage. The digital output, functioning as the controlling logic, reverses the polarity of the voltage across the coil, through a "Quadrant-Switching" circuit (Fig. 2). The experiment will not start until the field is stabilized and a proper quadrant is set.

Thus, a field rotation can be achieved with this apparatus without physically altering the sample orientation. A series of experiments with field orientations covering an entire hemisphere can be easily carried out. It is further proven to be very useful in pinpointing the molecular symmetry axes within the laboratory frame [4]. This is a potentially valuable tool to sort out the complicated HFI within the field range where electronic Zeeman energy and HFI have comparable magnitude.

Magnetic field is monitored with an F.W. Bell 620 Gaussmeter. At ZF, the field uncertainty is ± 5 μT, which is limited by the Gaussmeter precision. The field uncertainty is $\pm$ 5% when it is larger than 0.1 mT. This larger uncertainty arises from the uncertainty in coil resistance which is mainly caused by the ambient temperature fluctuation.

3. Results and discussion

The spin Hamiltonian for the $S = 1$ system is expressed as follows:

$$H = -XS_X^2 - YS_Y^2 - ZS_Z^2 + \sum_k S \cdot A_k \cdot I_k + g\beta B \cdot S + g_n\beta_n B \cdot I_k, \quad (3)$$

where X, Y, and Z are the zero-field splitting parameters, A_k is the kth HFI tensor element, and the last two terms are the Zeeman energy of the electron and nuclear spins. There are three possible ZF transitions. We shall report the T_x–T_z and T_y–T_z transitions of the pentacene triplet in mixed crystals and powdered solids to illustrate the utilities of this field rotation technique in this communication. Previously, we reported the T_x–T_z transition in ZF arises from the coupling of the oscillating field B_1 with the magnetic moment along the y-axis, $\mu_y(t)$, associated with S_y operator obeying the following equation ([1]),

$$\mu_y(t) = \text{Tr}[S_y\rho(t)] = -(P_z - P_x)\sin(2\theta_P)\sin[(Z - X)t]. \quad (4)$$

Similarly, for the T_y–T_z transition, we have,

$$\mu_x(t) = \text{Tr}[S_x\rho(t)] = -(P_y - P_z)\sin(2\theta_P)\sin[(Y - Z)t], \quad (5)$$

where $\rho(t)$ is the density matrix and P_j is the population rate of the T_j spin state. The signal intensity is expected to be proportional to the population difference between two spin sub states and the pulse rotation angle as given in Eqs. (4) and (5). We shall discuss the effects of small external field on the spectral patterns of single crystals and powdered solids, and those of site symmetry in single crystals.

3.1. Crystal versus powder

In single crystal experiments, the crystal was mounted on a xy-wedge where one of the pentacene molecules will have its molecular z-axis parallel to the Lab **Z** axis. Note

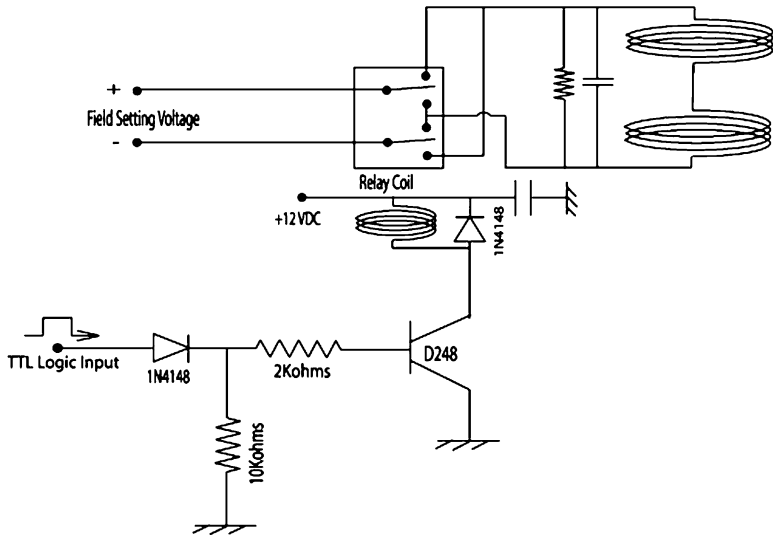

Fig. 2. Computer controlled quadrant switch circuit diagram. Three modules, each as illustrated above, are used to control the electric currents in each coil sets.

that B_1 of the microwave is applied parallel to the Lab **Z** axis. The powder samples were a collection of crushed ultra fine powder. In ZF, the full width at half maximum (FWHM) of single crystal spectra are about 400 and 700 kHz for PDPT and PHPT, respectively. But the FWHM of powder samples are 100 kHz broader for PDPT and PHPT than those of single crystals. The comparison is shown in Fig. 3A for PHPT and Fig. 3B for PDPT (dotted lines for single crystal, and solid line for powder). The difference in the spectral breadths of PDPT and PHPT is attributed to the second order HFI due to the difference of gyramagnetic ratio between proton and deuteron ($\gamma_H/\gamma_D = 6.5$).

In principle, we should not observe any spectral difference in single crystals and powder samples in ZF. The observed spectral broadening in powder samples may arise from some microscopic domains of fractured crystalline with pentacene molecules subject to stress and strain during the crushing of crystals and give rise to different ZFS. This is consistent with our previous observation where the measured ZFS of pentacene is very sensitive to the environmental conditions, such as different host crystal and temperature [1]. In an ensemble of randomly oriented molecules of powdered solids, the application of an oscillating B_1 field, in coupling with the magnetic moment $\mu_y(t)$ for the T_x–T_z transition will selectively excite only those molecules with their y-axis parallel to the B_1 field. Consequently, an orientation distribution of molecular y-axis of the powder sample with respect to the B_1 field will give rise to a statistical distribution of pentacene with slightly different sets of ZFS which will yield a broader spectral line.

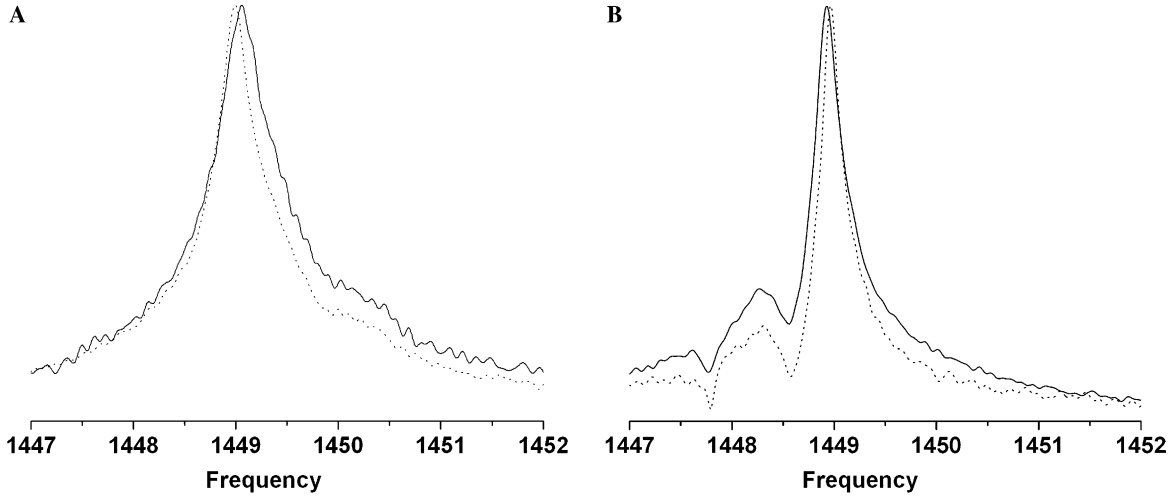

Fig. 3. The spectra for the T_x–T_z transition for powdered solids and single crystals at ZF: (A) PHPT powdered solids (solid line) and crystals (dotted line), (B) PDPT powdered solids (solid line) and crystals (dotted line).

In Fig. 4A, we display the spectral patterns of PHPT single crystal when an external field of 0.6 mT was applied across the unique molecular x-axis. Note that the x-axes of the two inequivalent molecules in the crystal are parallel to each other. In Fig. 4B, we show the powder spectra of PHPT at 0.7 mT where we observe no orientational anisotropy within the Lab **XY** plane (dotted line for **X** and dash line for **Y**). The line became 300 kHz broader and the peak frequency shifted 140 kHz higher when the external field was applied along the Lab **Z** axis (solid line). Similar spectral patterns were also observed in PDPT powder samples in the NZF region. We note that the broadening and frequency shift of the spectral peak is apparent only when the B_0 magnetic field coincides with the Lab **Z** which is also parallel to the B_1 orientation. Here the effective field $(B_0 + B_1)$ is maximal along the Lab **Z** (the vertical axis). We attribute this effect to the microwave selectivity which can induce transition only on those molecules with their molecular y-axis parallel or nearly parallel to the Lab **Z**, and one observes greater Zeeman interaction in this set of observable molecules. The other two magnetic orientations (perpendicular to the Lab **Z**) will produce less Zeeman interaction and less spectral shift due to orientational distribution.

On the other hand, the single crystal spectra are highly dependent on the field orientation. We observed different spectral behavior for the T_x–T_z transition of PDPT crystals as a function of magnetic field for $B_0//x$ (Fig. 5A). We observed no HFI due to deuterons instead a spectral shift of 500 kHz at $B_0 = 1.0$ mT. This is reasonable on the account of its small γ_D. Detailed calculations will be published elsewhere [5] and briefly discussed in Section 3.3.

Furthermore, the spectra of the T_y–T_z transition of the PHPT crystal at 1.0 mT for B_0 applied within molecular yz plane is displayed in Fig. 6A. The variation of spectral patterns are very noticeable. To analyze the spectral parameters, we set the field along the molecular

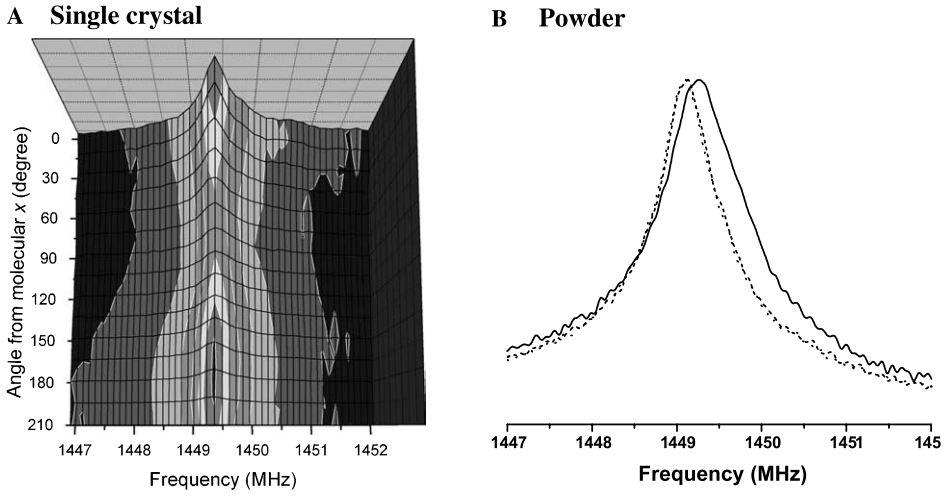

Fig. 4. The spectra for the T_x–T_z transition of PHPT: (A) contour map of single crystal at 0.6 mT for B_0 in the molecular xy plane (0° and 180° are for $B_0//x$), and (B) powdered solids at 0.7 mT for field along Lab X-axis (dotted line), along Y-axis (dash line), and along Z-axis (solid line). Note that the spectrum is broader and the frequency shifted higher when $B_0//B_1$//Lab Z.

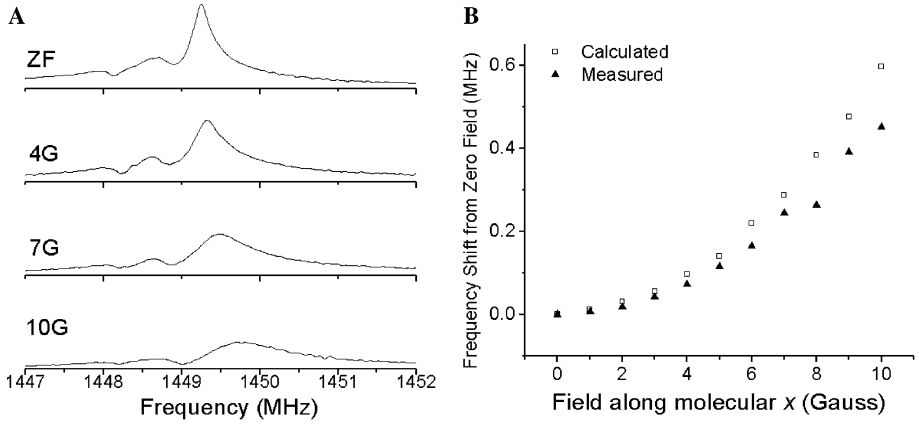

Fig. 5. The T_x–T_z transition of PDPT crystals: (A) as a function of magnetic field for $B_0//x$, and (B) the calculated frequency shifts based on Eq. (6).

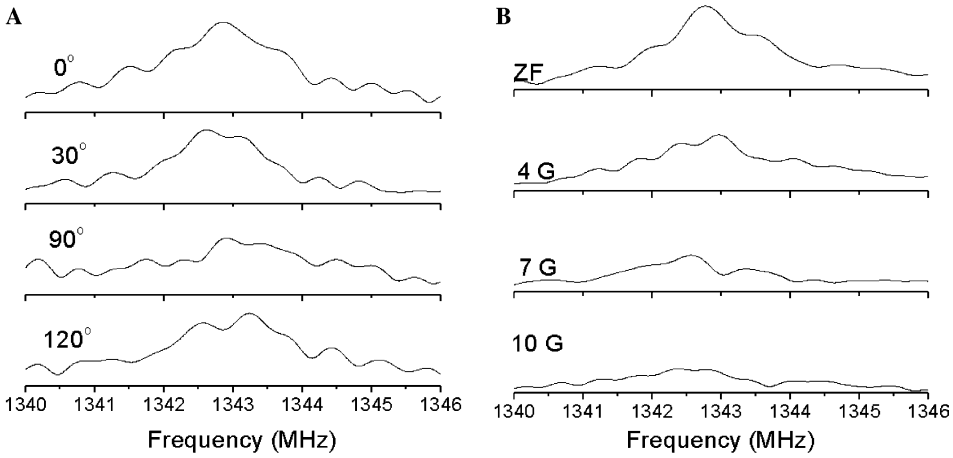

Fig. 6. The spectra of the T_y–T_z transition of PHPT crystals, (A) $B_0 = 1.0$ mT applied within molecular yz plane, and (B) B_0 along the molecular x-axis at various field strength.

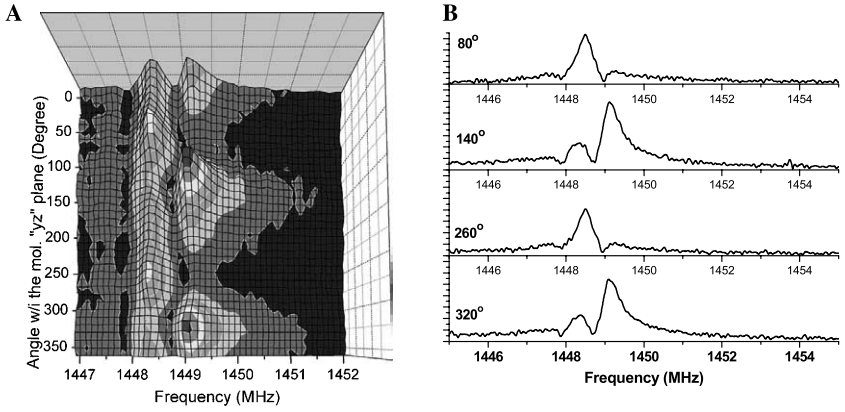

Fig. 7. The T_x–T_z transition of PDPT crystals at 0.4 mT with field oriented within the yz plane of the pentacene molecule: (A) 3D and (B) 2D pattern. The maxima of the two peaks are 60° apart.

x-axis and varied the field strength. The results are shown in Fig. 6B. We note the poorly resolved quintet spectral structure observed in ZF becomes resolved into septet with a splitting of 0.6 MHz when $B_0 = 0.4$ mT. We also notice that the spectral pattern is very similar to the HFI patterns observed in the x-band ESE experiments when $B_0 // x$ [6]. We therefore attribute this spectral splittings and patterns to proton HFI (see Section 3.3 for further discussion).

3.2. Site symmetry

Since pentacene molecules in the monoclinic p-terphenyl crystal could have two inequivalent orientations at room temperature, the crystal mounted on the xy-wedge will have the molecular x and y axes of one of the pentacene molecules lying on the Lab **XY** plane, and one of the molecular z-axes parallel to the Lab **Z** axis. Note that the molecular x axes of these two inequivalent molecules are parallel to each other, but their y and z molecular axes are not parallel to each other. So experimentally we started off by searching for this unique molecular x axis.

The measured spectra for PDPT single crystal mounted on the xy-wedge in the NZF region along all orientation should provide the needed information. When a field of 0.4 mT was applied along the molecular x axis, the peak frequency of the T_x–T_z transition was observed to shift by 75 kHz with the maximum signal intensity. On the other hand, when the field was applied along the molecular z axis ($B_0 // B_1$), the peak frequency is the highest with minimum signal intensity. The observed frequency shifts are consistent with the calculated values (see below).

Once we determine the molecular x axis, the plane perpendicular to that axis should be the molecular yz plane. Fig. 7A displays the 3D contour map at 0.4 mT in the yz plane of PDPT with 10° angular resolution. A few 2D spectral patterns are also shown in Fig. 7B to aid visual inspection. The contour map reveals two maxima which are 60° apart as shown in Fig. 7A. Assuming the pentacene molecule replaces p-terphenyl

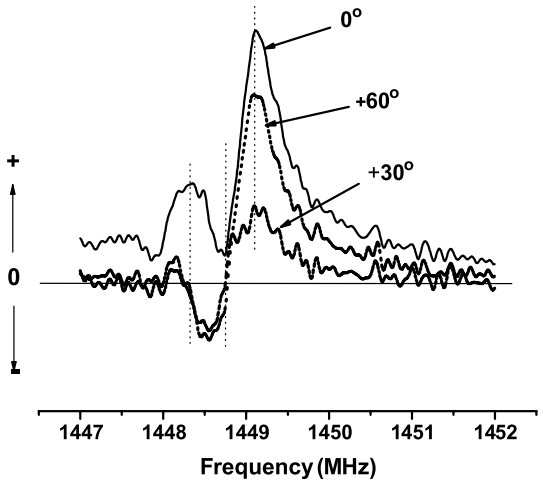

Fig. 8. The difference spectra of the T_x– T_z transition of PDPT single crystal at 0.4 mT at three orientation (from Fig. 7A). The reference spectrum is for $B_0//y$ (0°) and the other two difference spectra shown are for 30° and 60° moving away from the y axis.

host molecule substitutionally in the crystal lattice, then the observation that the yz plane of the pentacene takes either of these two orientations (sites) that are 60° apart is in agreement with the crystal structure of p-terphenyl solids [2,3].

We further apply the following subtraction procedure to examine the detailed spectral changes as we step a magnetic vector along different orientations: (1) identify a spectrum corresponding to a unique axis (e.g., y-axis, designated as spectrum A), and (2) subtract spectrum A from the new spectrum obtained at a different angle. The difference spectrum, however small, will represent the spectral change at the new orientation deviated from that unique axis. A few difference spectra for PDPT single crystals at 0.4 mT in the molecular yz plane are displayed in Fig. 8 (cf. Fig. 7). The negative intensity in the difference spectrum indicates that a shift of integrated intensity to another spectral region and zero intensity in the difference spectrum means two spectra are identical. This is a very sensitive technique that allows us to detect the spectral changes as a function of other variables, such as orientation and temperature.

3.3. Second order perturbation calculations

The eigenvalues of the $S = 1$ system can be calculated from the spin Hamiltonian given in Eq. (3). Since nuclear Zeeman effect is on the order of kHz in NZF range, it will be neglected in our calculation. There are 14 protons in the pentacene molecule. Hence, the exact solution to Hamiltonian (3) involves solving (3×2^{14}) dimensional matrix. Pentacene molecule has D_{2h} symmetry with four inequivalent protons, which reduces the problem to eight matrices of about 6000 dimensional. Given the difficulty of the problem, we treat the HFI and Zeeman interaction in NZF as the second order perturbation, and then the T_x–T_z transition energy shift for a given configuration of nuclear spins can be calculated by the following equation, similar to a previous treatment in NZF experiments [7]:

$$\Delta E = \frac{(\gamma B_z + \sum_{k=1}^{4} \pm\frac{1}{2}A_{kzz})^2}{X-Y} + \frac{2(\gamma B_y + \sum_{k=1}^{4} \pm\frac{1}{2}|A_{kyy} + iA_{kxy}|)^2}{X-Z} + \frac{(\gamma B_x + \sum_{k=1}^{4} \pm\frac{1}{2}|A_{kxx} + iA_{kxy}|)^2}{Y-Z}, \quad (6)$$

where γ is electron gyro magnetic ratio ($g\beta$); B_x, B_y, and B_z are magnetic field strengths along molecular principal axes x, y, and z; A_{kxx}, A_{kxy}, A_{kyy}, and A_{kzz} are HFI tensor elements for the kth proton, where we neglect the contribution from all off-diagonal terms except A_{kxy} as evidenced from the previous ENDOR study of the pentacene triplet state [8].

We calculated the spectral shifts of the T_x–T_z transition for PDPT crystals at various magnetic field for $B_0//x$ based on Eq. (6). The calculated frequency shifts of the T_x–T_z transition agree with the observed value within experimental uncertainty. The results are given in Fig. 5B. The calculated frequency shifts at 0.4 mT along x, y, and z are 86, 165, and 634 kHz, respectively. For $B_0//x$, the calculated value of 86 kHz is slightly larger than the observed value of 75 kHz, which may arise from the field uncertainty (5%) and the measurements may be taken at slightly different ambient temperature. Note that the ZF transition frequency is very sensitive to the sample temperature [1].

For the T_y–T_z transition of PHPT crystal displayed in Fig. 6, we observed a well resolved structure in the presence of an external field as low as 0.4 mT. First, we must recognize the fact that we applied the S_x operator to induce the transition (see Eq. (5)), the newly created magnetic moment $\mu_x(t)$ by the B_1 field could effectuate A_{xx} component (the largest proton HFI tensor element along x-axis is at the center ring, −16.52 MHz [8]) which could give rise to the first order HFI. The magnitude of the first HFI splitting is proportional to the magnitude of the coupling matrix elements between spin sub states. Detailed theoretical treatments are in progress and will be published elsewhere.

Acknowledgments

This work was supported by a PRF grant administered by the American Chemical Society (36970). We wish to thank Professors Ronald Lovett and Sam Weissman for helpful discussion.

References

[1] T.C. Yang, D.J. Sloop, S.I. Weissman, T.-S. Lin, Zero-field magnetic resonance of the photo-excited triplet state of pentacene at room temperature, J. Chem. Phys. 113 (2000) 11194–11201.

[2] J.L. Baudour, Y. Delugeard, H. Cailleau, Structural transition in polyphenyls. I. Crystal structure of the low temperature phase of *p*-terphenyl at 113 K, Acta Crystallogr. B 33 (1976) 150–154.
[3] J.L. Baudour, H. Cailleau, W.B. Yelon, Structural phase transition in polyphenyls. IV. Double-well potential in the disordered phase of *p*-terphenyl from neutron (200 K) and X-ray (room temperature) diffraction data, Acta Crystallogr. B 33 (1977) 1773–1780.
[4] S.M. Neugebauer-Crawford, D.S. Tinti, Isotope effects and proton hyperfine interactions in the lowest $^3n\pi$ state of substituted benzaldehydes, J. Chem. Phys. 103 (1995) 9138–9145.
[5] Jun Lang, Pulsed EPR studies of pentacene triplet state in zero and near zero magnetic field from 300 K to below phase transition temperature of *p*-terphenyl, PhD Thesis, Washington University, May 2005.
[6] J.-L. Ong, D.J. Sloop, T.-S. Lin, Temperature dependence studies of the paramagnetic properties of the photoexcited triplet state of pentacene in *p*-terphenyl, benzoic acid, and napthalene crystals, J. Phys. Chem. 97 (1992) 7833–7838.
[7] C.A. Hutchison Jr., J.V. Nicholas, G.W. Scott, Magnetic resonance spectroscopy of triplet-state organic molecules in zero external magnetic field, Chem. Phys. 53 (1970) 1906–1917.
[8] T.-S. Lin, J.-L. Ong, D.J. Sloop, H.-L. Yu, Spin Echo ENDOR Studies of Organic Triplets at Room Temperature, in: C.P. Keijzers, E.J. Reijerse, J. Schmidt (Eds.), Pulsed EPR: A New Field of Applications, North Holland, Amsterdam, 1989, pp. 191–195.